bioRxiv preprint doi: https://doi.org/10.1101/578963; this version posted March 15, 2019. The copyright holder for this preprint (which was not certified by peer review) is the author/funder, who has granted bioRxiv a license to display the preprint in perpetuity. It is made available under a CC-BY 4.0 International license.

Dynamic metabolic profiles of marine macroalga *Ulva prolifera* during fragmentation-induced proliferation

Yanli He[1,2] Yanhui Wang[2] Chaoyang Hu[1] Xue Sun[1] Yahe Li[1] *Nianjun Xu[1]

[1] Key Laboratory of Applied Marine Biotechnology of Ministry of Education, School of Marine Science, Ningbo University, Ningbo 315211, China;

[2] Zhejiang Pharmaceutical College, Ningbo 315211, China.

Abstract

Ulva prolifera, a type of marine macroalgae, is the causative species behind green tides mainly in the Yellow Sea and adjacent regions, nevertheless, it can be used as food or animal feed in South China. The vegetative fragments of *U. prolifera* are an important seed source for successive green tide blooms. Fragmentation shortens the transition time from the vegetative state to the reproductive state. However, the translation of the algal metabolites during gametogenesis was far from well understood. In this study, the dynamic metabolic profiles of *U. prolifera* thallus during fragmentation-induced proliferation were investigated using non-targeted metabolomics approach in a time series of experiments in June 2017. After a 30 min low temperature shock, fragmentation induced a reproductive response of 91.57% of *U. prolifera* in 48 h, whereas that was only 21.43% in the control group. A total of 156 chromatographic peaks were detected, and 63 metabolites were significantly

bioRxiv preprint doi: https://doi.org/10.1101/578963; this version posted March 15, 2019. The copyright holder for this preprint (which was not certified by peer review) is the author/funder, who has granted bioRxiv a license to display the preprint in perpetuity. It is made available under a CC-BY 4.0 International license.

changed in *U. prolifera* during reproduction. The results of the Kinetic metabolic pattern showed that the fragments not only induced the formation of sporangium, but also complicated their metabolites accumulation. During fragmentation-induced proliferation, *U. prolifera* consumed different sugars at different time points. γ-aminobutyric acid (GABA), glutamic acid, gallic acid, and malic acid may play important roles in germ cell formation and release of *U. prolifera*, whereas n-hexanol, 2-methyl-3-phenylindole, and 3-indoleacetonitrile may be beneficial in biotic stress resistance. Compared with the control group, the metabolites, such as alcohol and organic acid, also showed significant difference with the photoperiod at the initial stage of proliferation (before 60 h). In conclusion, that the metabolites including sugars, organic acids, and alcohol changed with different photoperiod may be the strategy for *U. prolifera* to cope with adverse environment and rapid proliferation.

Funding This study was financially supported by the National Natural Science Foundation of China (41876181; 41276122; 41606129), the Key Program of Natural Science Foundation of Zhejiang Province (LZ17D060001), Foundation of Zhejiang Pharmaceutical College (ZPCSR2014010) and Program of Science and Technology Bureau of Ningbo Municipality (2017D10019). This research was also sponsored by the K.C. Wong Magna Fund in Ningbo University.

Conflict of interest Authors declare that they have no conflict of interest.

* E-mail：xunianjun@nbu.edu.cn

Introduction

bioRxiv preprint doi: https://doi.org/10.1101/578963; this version posted March 15, 2019. The copyright holder for this preprint (which was not certified by peer review) is the author/funder, who has granted bioRxiv a license to display the preprint in perpetuity. It is made available under a CC-BY 4.0 International license.

Marine macroalgae are potential sources of oil, food, and valuable compounds[1]. *Ulva* spp. are attractive models for understanding plant growth, development, and evolution, but they can cause severe ocean green tides. *Ulva* species generally have complex life cycles, which alternate between diploid and haploid generation, and exhibit parthenogenetic development of gametes. The germ cells of *Ulva* species are transformed directly from vegetative cells [2]. This transformation is caused by external factors. Tissue fragmentation is considered to be an important factor in inducing this transformation and reproduction quickly [3]. Fragments significantly increase the sporulation rate of *U. mutabilis* from 15.8% to 80.0% [4]. Within 2-3d after fragmentation, the reproduction of *U. pertusa* was induced [2]. Gao et al (2010). found that almost all *U. prolifera* fragments with a diameter of 0.5 mm were transformed into sporangium, whereas the sporangium in larger fragments was only formed by marginal and sub-marginal cells [5].

The mechanism of fragmentation-induction has been preliminarily considered that cutting destroyed cell walls and the additional cell-matrix structure, making it easier for algal segments to filter out inhibitors, thus removing the regulatory barriers to reproduction [2]. The gametogenesis of mature blades can be artificially induced by mincing the thallus into single mono-layered fragments and by washing-out of the sporulation inhibitors[6-8]. Previous studies showed that fragmentation-induction only improved the conversion rate of *Ulva* sporangium, and *Ulva* filaments can also be transformed into sporangium under the same culture conditions[4,5]. Cell differentiation is a popular topic in macroalga research[9,10]. However, the changes

bioRxiv preprint doi: https://doi.org/10.1101/578963; this version posted March 15, 2019. The copyright holder for this preprint (which was not certified by peer review) is the author/funder, who has granted bioRxiv a license to display the preprint in perpetuity. It is made available under a CC-BY 4.0 International license.

of the algal metabolites in space and time are far from well understood. Thus, we aimed to identify changes of the chemical composition of the metabolome during gametogenesis of *Ulva prolifera*. The metabolomics is a powerful tool for the study on the metabolism and physiological functions of marine organisms including seaweed [11,12]. Several metabolomic studies on the growth and reproduction of plants have been conducted[13]. In recent years, studies on marine macrophytes such as *Ectocarpus*, *Porphyra*, and *Zostera* by GC-MS(gas chromatography-mass spectrometry) have provided a comprehensive understanding of the metabolic networks linked to photorespiration pathways, tricarboxylic acid cycle, glycolysis, and pentose phosphate pathway involved in the acclimatization to external stressors[13,14]. In this study, the metabolites of *U. prolifera* in both natural reproduction and fragmentation-induced reproduction at different time points were investigated, and the results may help in exploring the causes of the rapid formation of marine green tides.

Materials and methods

Culture conditions

Vegetative *U. prolifera* thalli were collected from Xuwen Seaweed Co., Ltd., Xiangshan County, Zhejiang Province, China (121°56′153, 29°05′065), in June 2017. The thalli were gently washed three times with sterile seawater and then rinsed thoroughly. Using a magnifying glass, the attached sediments, small herbivores, and epiphytes were removed with a brush. Afterward, the thalli were cultured in f/2

bioRxiv preprint doi: https://doi.org/10.1101/578963; this version posted March 15, 2019. The copyright holder for this preprint (which was not certified by peer review) is the author/funder, who has granted bioRxiv a license to display the preprint in perpetuity. It is made available under a CC-BY 4.0 International license.

medium with the following specific parameters: light intensity, 70 mmol photons m^{-2} s^{-1}; temperature, 25 ± 1 °C; and light:dark cycle, 12 h:12 h in an intelligent illumination incubator (GXZ-280 C, Ningbo Jiangnan Instrument, China) at a salinity of 22 ± 1 for acclimation for about a month before the experiments. Ampicillin (100 $mg.L^{-1}$), gentamycin (50 $mg.L^{-1}$) and GeO_2 (0.3 mg L^{-1}) were added to suppress the growth of bacteria and diatoms[15] The medium was aerated and refreshed every other day. Unless otherwise specified, the following experiments were performed under the same conditions. The formal experiment began after 20 - 25 d of domestication.

Sample treatments

Treatment group: *Ulva* thalli were harvested at morning and cut into small single-layered fragments (200 - 500 cells fragment) using a Zyliss ® Smart Clean Food Chopper. Two grams of fresh algae fragments were cultured in a 3000 mL flask containing 2500 mL of sterile artificial seawater. Control groups: two grams of fresh uncut vegetative thalli was cultured under the same conditions. Both were pre-cultured at 4 °C for 30 min in a refrigerator and performed with six duplicates. Samples were collected at culture times of 12, 24, 36, 48, 60, 72, 96, and 120 h, and the media were reduced accordingly to maintain the same culture density.

Microscopic observations and counting methods

The formation and release of *U. prolifera* germ cells were observed under an AOTE BK5000 microscope equipped with a Cool SNAP digital camera system. Seven microscopic fields of view were randomly observed in each selected fragments or

bioRxiv preprint doi: https://doi.org/10.1101/578963; this version posted March 15, 2019. The copyright holder for this preprint (which was not certified by peer review) is the author/funder, who has granted bioRxiv a license to display the preprint in perpetuity. It is made available under a CC-BY 4.0 International license.

uncut thalli. During the maturation process, the germ cell sporangium and released germ cell sporangium were imaged to count their numbers. The percentage of mature germ cell sporangium and the formation and release rates were calculated using the following equations: $Sp = (Sm / At) \times 100\%$, $Rp = (Ss/At) \times 100\%$,where S_p represents the percentage of mature sporangium, S_m represents the mature sporangium, R_p represents the percentage of released germ cell cysts per unit of thalli, S_s represents the germ cell cysts that were released (in μm^2), and A_t represents the number of germ cell cysts in the whole field under the microscope.

Metabolite extraction and GC-MS analysis

Extraction

Sample materials (20mg±2mg) were put in 2mL Eppendorf tube. One metal or zirconia ball was added in every tube. 700µL 100% methanol and 5.75 µL Stock ribitol (Sigma-Aldrich, München, Germany, 0.2 mg/mL Stock in Water) were added, then vortexed for 15 seconds. Following by homogenized with the Retschmühle for 3 min at 25 Hz. Centrifuged for 10 min at 14000 rpm and take 600 µL from the upper phase into 2mL fresh Eppendorf tubes, then 300µL $CHCl_3$ added and mixed it slowly. After that, 750 µL H_2O was added in and vortex 15 sec. Subsequently, centrifuged 10 min at 14000 rpm and 150 µL upper phase (polar phase) was taken into 1.5mL Eppendorf tubes. Finally, all the extracts were dried in a speed vac for at least 3 h in normal temperature condition.

Derivatization

bioRxiv preprint doi: https://doi.org/10.1101/578963; this version posted March 15, 2019. The copyright holder for this preprint (which was not certified by peer review) is the author/funder, who has granted bioRxiv a license to display the preprint in perpetuity. It is made available under a CC-BY 4.0 International license.

After evaporation of the solvent, 40 µL of methoxyamine hydrochloride (Sigma-Aldrich) solution (20 mg/mL) in pyridine was added for derivatization and incubated at 60°C for 1 h. Subsequently, 50 µL of N-Methyl-N-(trimethylsilyl) trifluoroacetamide (Macherey-Nagel, Düren, Germany) was added to each sample and incubated at 40 °C for 1 h, then transferred 100 µL into sample vials and analyzed directly by GC-MS.

GC-MS analysis

The metabolites were detected using the Trace 1300/ITQ 900 GC-MS system (Thermo Fisher Scientific, USA, Serial No.13005). GC-MS analysis were conducted as previously reported [16] with slight modifications. The samples were injected with a 1300 autosampler equipped with a 10-µL tapered, fixed needle, polytetrafluorethylene (PTFE)-tipped plunger syringe. The column and all spare parts were purchased from Thermo Fisher Scientific (Thermo Fisher Scientific, USA). The GC parameters for the analysis were as follows: The inlet temperature was 250°C, EI ion source temperature was 230°C, high-purity helium (99.99%) as the carrier gas, an amount of 1 µL sample was injected with the splitless mode. The temperature was initially set at 60 °C for 2 min, then increased by 10 °C min^{-1} up to 150 °C and held for10 min. Then, the temperature rised to 250 °C at 15 min^{-1} and held for 20 min. MS was performed with a full-scan mode with MS range from 0 to 550 (m/z).

Data analysis

Compounds were identified based on the ratio and relative abundance of the National Institute of Standards and Technology database (NIST) and MassBank website

bioRxiv preprint doi: https://doi.org/10.1101/578963; this version posted March 15, 2019. The copyright holder for this preprint (which was not certified by peer review) is the author/funder, who has granted bioRxiv a license to display the preprint in perpetuity. It is made available under a CC-BY 4.0 International license.

(http://www.massbank.jp/) according to mass/charge. Statistical analyses were performed in MetaboAnalyst 3.0 (http://www.metaboanalyst.ca/) according to its protocol (Linting and Meulman 2011). “Normalization by internal standard ribitol” was chosen for sample normalization, “None” for data transformation, and “Auto scaling” for data scaling. Principal component analysis (PCA) and orthogonal partial least squares discriminant analysis (OPLS-DA) were performed in the SIMCA-P 13.0 software package using Auto scaling. Two-sided T-test, one-way ANOVA, two-way ANOVA, post-hoc analysis, and ANOVA simultaneous component analysis (ASCA) were performed in MetaboAnalyst 3.0 (http://www.metaboanalyst.ca/) according to its protocol[17]. “Auto scaling” was selected as the data scaling method for all analyses. The two-way ANOVA type used was “within subject ANOVA.” Statistical significance was considered at $P < 0.05$, and the false discovery rate was used for multiple testing correction. For ASCA, the alpha and leverage thresholds were set as 0.05 and 0.9, respectively. Figures were edited with Adobe Illustrator CS5 for better resolution.

Results

Microscopic observation of the germ cell sacs formation

As shown in Fig. 1, the mature germ cell sac first appeared on the edge of the cut algae at 24 h, but most of the cells remained in a vegetative state at 60 h in the control group. At 48 h, nearly all of the vegetative cells (91.57%) (Table 1) in the treatment group were transformed into germ cell sacs, and the germ cell sacs that matured early

bioRxiv preprint doi: https://doi.org/10.1101/578963; this version posted March 15, 2019. The copyright holder for this preprint (which was not certified by peer review) is the author/funder, who has granted bioRxiv a license to display the preprint in perpetuity. It is made available under a CC-BY 4.0 International license.

178 at the edge began to release. However, only 9.57% of the vegetative cell
179 transformation germ cell sacs until 60 h in the control group (Table 1). At 72 h, nearly
180 all of the vegetative cells (98.29%) were transformed into mature germ cell sacs in the
181 treatment group, meanwhile, 20.43% of the algae were transformed into germ cells
182 (Table 1) in the control group. At 96 h, almost all of the cells were transformed into
183 mature germ cell sacs. Moreover, germinated seedlings appeared in the treatment
184 group. However, only 4.28% germ cell sacs were released in the control group
185 although most of the vegetative cells were transformed into germ cell sacs (120 h,
186 Fig.1).

187

188 **Fig. 1.** Microscopic observation of the transformation of *U. prolifera* from the vegetative state to the
189 reproductive state after cutting (left: uncut(control); right: cut (treatment) 12h, 24h, 36h, 48h, 60h, 72h,
190 96h, 120h) (in treatment 48h: a, b, c, d, represent vegetative cell; mature germ cell sac; released germ
191 cell sac; and released gametophytes/sporophytes respectively; in treatment 120h: e represents
192 germinated seedling) , the scale bars represent 20 μm.

193

194 **Table 1.** Transformation of *U. prolifera* from vegetative cells into germ cell sac and their release rate.

[a] percentage of mature germ cell sporangium

[b] release rates of germ cell sporangium

[c] average of six tests

195

196 # Analysis of metabolite profiles

bioRxiv preprint doi: https://doi.org/10.1101/578963; this version posted March 15, 2019. The copyright holder for this preprint (which was not certified by peer review) is the author/funder, who has granted bioRxiv a license to display the preprint in perpetuity. It is made available under a CC-BY 4.0 International license.

197 To investigate the metabolic profiles of *U. prolifera* during fragmentation-induced
198 proliferation, both the filament and fragments at 12, 24, 36, 48, 60, 72, 96, and 120 h
199 were collected and subjected to metabolic profiling analysis based on GC-MS.
200 Smoothing and baseline correction was performed prior statistical analysis. After the
201 background subtraction , the impure peaks due to column material loss or impurity
202 caused by the sample preparation process were removed, only m/z values with
203 signal-to-noise ratio more than 10 were picked out. As a result, 156 chromatographic
204 peaks were detected. The GC-MS data were eventually organized into
205 two-dimensional matrices, including observed values (samples) and variables (peak
206 intensities). PCA was subsequently performed on the 156 metabolites to obtain
207 overall patterns within the kinetic metabolic patterns and induction methods of
208 reproducing *U. prolifera*. The first principal component (PC1), accounting for 27.9%
209 of the total variance, reflected time-dependent *U. prolifera* reproduction, and samples
210 from treatment and control groups were gathered at the same time point (Fig. 2). The
211 results indicated that the developmental time affected *U. prolifera* metabolites more
212 than the induction method did. The second principal component (PC2) accounted for
213 15% of the total variance. The samples of the treatment and control groups at the
214 same time points were all distinguishable in PCA plots, indicating that the metabolites
215 with different treatments of *U. prolifera* were different at the same developmental
216 times.

217

218 **Fig. 2** PCA of *U. prolifera* during its fragmentation-induced proliferation (Colors represent different

bioRxiv preprint doi: https://doi.org/10.1101/578963; this version posted March 15, 2019. The copyright holder for this preprint (which was not certified by peer review) is the author/funder, who has granted bioRxiv a license to display the preprint in perpetuity. It is made available under a CC-BY 4.0 International license.

219 treatment times, boxes (□) represents the control group, and cycle (○) represents the treatment group;
220 n=6).

221

222 PCA provides a high-level summary of the main patterns of data variance. Detailed
223 metabolite abundance profiles can be obtained from the visualization of metabolomic
224 data based on heat map. The changes of metabolites in the cut and uncut thallus over
225 time are mainly the same. Of note, these metabolites exhibit opposite trends at the 36
226 and 48 h time points with respect to the treatment and control groups (Fig. 3).

227

228 **Fig. 3** Heatmap analysis, combined with HCA, of the metabolites in *U. prolifera*
229 fragmentation-induced proliferation (treatment and control groups) during 12-120 h (n=6).

230

231 Two-way repeated measures (within subjects) ANOVA was then utilized to analyze
232 which factors (treatment, developmental time, and their interaction) caused the
233 variation of each metabolite. The abundance of 63, 32, and 58 metabolites was
234 affected by treatment, developmental time, and their interaction, respectively (Fig. 4).

235

236 **Fig.4** Two-way repeated measures (within subjects) ANOVA of metabolites in *U. prolifera*
237 fragmentation-induced proliferation during 12 -120 h.

238

239 ASCA was performed to determine the trends of treatment methods, developmental
240 time, and their interaction patterns[17]. The time score plots based on component 1

bioRxiv preprint doi: https://doi.org/10.1101/578963; this version posted March 15, 2019. The copyright holder for this preprint (which was not certified by peer review) is the author/funder, who has granted bioRxiv a license to display the preprint in perpetuity. It is made available under a CC-BY 4.0 International license.

(45.21% of variation explained) of the corresponding model demonstrated a decrease in scores from 12 h to 36 h, then increased at 48 h, then decreased from 48 h to 60 h, and final increased until 120 h (Fig. 5a). The treatment score plot showed that different dispose types differed in their PC1 scores, with the treatment and control groups having the lowest and highest scores, respectively (Fig. 5b). Component 1 of the interaction effect obviously exhibited opposite trends at 48 h between the treatment and control groups, while the same trend was observed at other times (Fig. 5c).

Leverage/squared prediction error (SPE) plots were made to correlate the metabolic features with the experimental factors[17]. The leverage evaluates the importance of the metabolite to the model, and SPE tests the fitness of the model for particular metabolites. Metabolites with high leverage SPE, which contribute significantly to the model, were chosen as well-modeled metabolites. In this way, 63 metabolites which were affected by treatment were analyze by SPE, a total of 31 metabolites were well modelled, including 3 alcohols, 5 amino acids, 11 organic acids 6 sugars and 6 other kinds metabolites (Table S1). Twelve well-modeled metabolites, including six organic acids (cyclohexylacetic acid, gentisic acid, octadecanoic acid, 2,3-dihydroxybenzoic acid, stearic acid, palmitic acid), two kinds of alcohol (isofucosterol and 2-naphthol), one amino acid (valine) and two other kinds of metabolites (tryptamine and 5-nonanone), were determined based on the major pattern of time (Fig. 5d and Supplementary Table S1). Their levels sharply declined from 0 h to 24 h in the filament and its fragments. Then, they increased at 36 h, decreased at 48

bioRxiv preprint doi: https://doi.org/10.1101/578963; this version posted March 15, 2019. The copyright holder for this preprint (which was not certified by peer review) is the author/funder, who has granted bioRxiv a license to display the preprint in perpetuity. It is made available under a CC-BY 4.0 International license.

h, and peaked at 96 h. Eight metabolites, including glycolic acid, glycerol, alanine, valine, arabinose, norvaline, chloroacetic acid allyl ester, and ribose, were well modeled by treatment method (Fig. 5e and Supplementary Table S1). Eleven metabolites, including fructose, allose, ribose, glycerol, cysteamine, galactose, ribulose-5-phosphate, ascorbic acid, 3-indoleacetonitrile, methylmalonic acid, and malic acid, were well modelled (Fig. 5f and Supplementary Table S1) based on the interaction, and their levels varied between the filament and its fragments.

Fig.5 ANOVA-simultaneous component analysis (ASCA) of *U. prolifera* during its fragmentation-induced proliferation.

Metabolic difference analysis

To simplify the information and obtain maximal covariance among metabolite levels during proliferation at different time points, OPLS-DA was applied. The OPLS-DA model, which was composed of one orthogonal component and one prediction component, generated the explained variation values R2X (cum) > 0.82 (except at 96 and 120 h where the R2X values were 0.482 and 0.44) and R2Y (cum) > 0.966 and the predictive capability Q2 (cum) > 0.753 at all six time points (Fig. 6). These high-value parameters indicated the excellence in modeling and prediction with good discrimination between the fragmentation-induced proliferation and natural proliferation of *U. prolifera* at each time point before 96 h because the model parameters (>0.5) are considered to be satisfactory in explanatory and predictive

bioRxiv preprint doi: https://doi.org/10.1101/578963; this version posted March 15, 2019. The copyright holder for this preprint (which was not certified by peer review) is the author/funder, who has granted bioRxiv a license to display the preprint in perpetuity. It is made available under a CC-BY 4.0 International license.

285 capabilities [18].

286 Based on a variable importance in projection (VIP) threshold (VIP > 1) from the
287 200-fold cross-validated OPLS-DA models, a number of metabolites associated with
288 the distinction of metabolic profiles of fragmentation-induced proliferation and
289 natural proliferation and fragmentation-induced proliferation at each time point were
290 procured. The candidate metabolites from the OPLS-DA model, whose *P*-values are
291 less than 0.05 between fragmentation-induced proliferation and natural proliferation at
292 each time point tested using the T-test with fold threshold of > 2 or < 0.5, were further
293 selected as biomarkers (Table 2).

294 **Table 2.** Metabolic difference between cut and uncut groups of *U. prolifera* at each time point.

[a] *P*-value was calculated from T-test (two-tails) with a cutoff of 0.05.

[b] Ratio of relative metabolites at 24 and 12 h after cut.

[c] VIP was obtained from OPLS-DA with a threshold of 1.0.

[d] Comparison of relative content of metabolites in *U. prolifera* at each time point.

295

296

297 **Fig.6** OPLS-DA of the uncut and cut treatment of *U. prolifera* at different time points.

298

299 At 12 h, four metabolites, maltose, 2-methyl-3-phenylindole, 3-indoleacetonitrile, and
300 glutamic acid, were selected as biomarkers (Table 2). The levels of maltose
301 (12.23-fold), 2-methyl-3-phenylindole (2.78-fold), and 3-indoleacetonitrile (2.33-fold)
302 were significantly higher and the relative abundance of glutamic acid was

bioRxiv preprint doi: https://doi.org/10.1101/578963; this version posted March 15, 2019. The copyright holder for this preprint (which was not certified by peer review) is the author/funder, who has granted bioRxiv a license to display the preprint in perpetuity. It is made available under a CC-BY 4.0 International license.

303 significantly lower than that in the control group.

304 At 24 h, three metabolites, maltose, propanedioic acid ester, and trehalose, were
305 important in distinguishing between the treatment and control groups (Table 2). In the
306 treatment group, the relative contents of trehalose significantly decreased, however,
307 the relative content of maltose increased by 12.44-fold, and those of propanedioic acid
308 ester also significantly increased.

309 At 36 h, a total of 18 metabolites, including six kinds of acids, two kinds of alcohol,
310 one benzene derivative, one kind of lipid, six flavonoids, three lipids, two
311 carbohydrates, and six other kinds of metabolites, played important roles in separating
312 the treated and control groups. In the treatment group, the top five metabolites with
313 the highest fold values were n-hexanol, 5-nonanone, GABA, ethylmalonic acid, and
314 pinene. In particular, the relative contents of n-hexanol was 15.09-fold higher than
315 that of the control group. The levels of five metabolites, 1-iodo-4-nitrobenzene,
316 gentisic acid, succinic acid, 2-naphthol, and cysteamine, were significantly decreased
317 in the control groups, with cysteamine having the lowest level (0.09-fold).

318 At 48 h, eight metabolites, including six carbohydrates and two acids, were selected
319 as biomarkers (Table 2). Among them, the relative content of four kinds of
320 monosaccharides (galactose, ribose, allose, and fructose) and glycerol decreased by
321 0.39–0.03-fold compared with those of the control groups. The levels of malic acid
322 and ascorbic acid increased significantly by 9.61- and 6.05-fold, respectively.
323 However, the levels of maltose, glycerol, allose, galactose, ribose, and fructose
324 decreased.

bioRxiv preprint doi: https://doi.org/10.1101/578963; this version posted March 15, 2019. The copyright holder for this preprint (which was not certified by peer review) is the author/funder, who has granted bioRxiv a license to display the preprint in perpetuity. It is made available under a CC-BY 4.0 International license.

At 60 h, three metabolites, including glycerol, arabinose, and glutamic acid, changed significantly between the treated and control group. Their relative contents were all decreased in the fragmentation-induced proliferation groups. At 72 h, only two metabolites (maltose and n-hexanol) were selected as biomarkers.

However, at 90 h, four metabolites, malic acid, norvaline, isoflavone, and glucose, accumulated significantly in the treatment group. Meanwhile, the relative contents of seven kinds of metabolites, including arabinose (0.11-fold), maltose (0.14-fold), ribose (0.26-fold), fucose (0.42-fold), shikimic acid (0.09-fold), iditol (0.27-fold), and 5-nonanone (0.29-fold), sharply decreased.

At 120 h, malic acid and gallic acid increased, and urea decreased compared with those in the control group.

Kinetic metabolic pattern

In order to investigate the variation of the 31 metabolites well modelled by SPE, multivariate Empirical Bayes Analysis (MEBA), a time-course analysis method based on the MEBA statistic, which can evaluate the importance of features by Hotelling's T, was employed to identify the metabolites, with differential temporal profiles [19]. Twenty-three metabolites, which meet the following conditions: potential biomarker (Table 2), the Hotelling's T2 value > 100 and well-modelled according the analysis by ASCA are shown in Fig. 7 (n-hexanol, cyclohexylacetic acid, alanine and urea varied obviously with time but did not meet the above three conditions at the same time) (Table 3). The changes of four carbohydrate metabolites (ribose, fructose, allose, and galactose) with time were consistent: from 0 h to 36 h, their abundance varied

bioRxiv preprint doi: https://doi.org/10.1101/578963; this version posted March 15, 2019. The copyright holder for this preprint (which was not certified by peer review) is the author/funder, who has granted bioRxiv a license to display the preprint in perpetuity. It is made available under a CC-BY 4.0 International license.

between -1 and 0, and almost reached 4 at 48 h in the control group. Then, the abundance sharply decreased to nearly 0 at 72 h, while that of the treatment group was relatively stable (Fig. 7a and Table 3). This result was consistent with the heat map. Take maltose for example, its abundance in the control group decreased from 0 to -2.5 and then gradually increased until reaching the highest at 60 h, followed by slight fluctuation with the photoperiod and maintaining a value between 0 and 1 at 0–48 h. The change trend was the same as that in the treatment group. However, the abundance of maltose in the treatment group fluctuated slightly between 0 and 1 with the photoperiod at 48–96 h and then decreased to below 0 at 96–120 h (Fig. 7b and Table 3). In the treatment group, the relative content of the four alcohols was related to the photoperiod before 60h, and the relative content increased at night (without light) and decreased during the day (with light), after 60 h, the relative content gradually leveled off. In the control group, however, 36 h was a cutoff point, where the relative content increased before 36 h and then decreased gradually (except for glycolic acid, where the relative content decreased gradually from 12 h). Interestingly, the relative content of other six metabolites including three organic acids (gentistic acid, ascorbic acid and cyclohexyacetic acid), valine, 1-Iodo-4 nitrobenzen and cysteamine also showed this trend.

Table 3 Metabolites of *U. prolifera* which meet following conditions: potential biomarkers according OPLS-DA, well-modelled by SPE and the Hotelling's T2 value > 100.

bioRxiv preprint doi: https://doi.org/10.1101/578963; this version posted March 15, 2019. The copyright holder for this preprint (which was not certified by peer review) is the author/funder, who has granted bioRxiv a license to display the preprint in perpetuity. It is made available under a CC-BY 4.0 International license.

369 **Fig. 7** Metabolites MEBA of *U. prolifera* which meet following conditions: potential biomarkers
370 according OPLS-DA, well-modelled by SPE and the Hotelling's T2 value > 100.
371

372 Discussion

373 Fragmentation-induced spores play a vital role in the rapid accumulation of large
374 amounts of biomass and may be one of the most important factors in accelerating the
375 occurrence of green tides on the coast of Qingdao China [5]. In this study,
376 reproductive cells (nearly 90%) (Table1) appeared within 48 h after *U. prolifera* thalli
377 were cut into approximately 0.5 mm segments. It was consistent with the results of the
378 study on *U. mutabilis* [4]. Interestingly, almost all the cells (96.29%) in the
379 physiological state transformed into the reproductive state at 120 h in the control
380 group. It indicated that fragmentation-induction was not the determinant of *U.*
381 *prolifera* sporangium formation, but only a promoter. The metabolic profiles of the
382 treatment group differed significantly from that of the control group according to PCA
383 and OPLS-DA. Time-course analysis showed that the relative content trend of
384 carbohydrates, alcohols and organic acids was different in treatment group and control
385 group (Fig 7).
386

387 Different sugars response during germ cell formation

388 Sugar is mainly involved in the biosynthesis of sugar polymers, including starch and
389 cellulose, generation of energy (ATP), cross-talk in invertase-mediated sugar
390 signaling, and phytohormone control [20]. The content of monosaccharides in the

bioRxiv preprint doi: https://doi.org/10.1101/578963; this version posted March 15, 2019. The copyright holder for this preprint (which was not certified by peer review) is the author/funder, who has granted bioRxiv a license to display the preprint in perpetuity. It is made available under a CC-BY 4.0 International license.

391 treatment group was significantly lower than that in the control group at two time
392 points: 48 h (ribose, fructose, allose, and galactose) and 96 h (arabinose) (Fig. 3 and
393 6), the results were consistent with the kinetic metabolic pattern analysis (Fig.7a).
394 Meanwhile, the content of maltose was higher in the treatment group within 12 - 48 h
395 after cutting and then became similar to that in the control group (Fig.7b). The result
396 indicated that in the process of fragmentation-induction and natural proliferation, *U.*
397 *prolifera* consumed different sugars. Kaplan and Guy (2004) indicated that the
398 resultant maltose accumulation may function as a compatible-solute stabilizing factor
399 in the chloroplast stroma in response to acute temperature stress [21]. In this study,
400 the accumulation of maltose suggests that it was not only related to energy
401 metabolism during the spore formation of *U. prolifera*, but also related to the response
402 to mechanical injury.
403

404 Organic acids may be involved in the redox function and 405 osmotic regulation of *U. prolifera*

406 Compared with the control group, several organic acids accumulated, including
407 ethylmalonic acid (4.35-fold) at 24 h, malic acid (9.61-fold) and ascorbic acid
408 (6.06-fold) at 48 h, and gallic acid (7.07-fold) and malic acid (7.02-fold) at 120 h
409 (Table 2). During the process of transformation from vegetative to reproductive state,
410 the pigmentation deepens, the vacuole becomes smaller and then disappeared at
411 treatment 36 h and control 48-60 h (Fig.1). The accumulation of organic acids may

bioRxiv preprint doi: https://doi.org/10.1101/578963; this version posted March 15, 2019. The copyright holder for this preprint (which was not certified by peer review) is the author/funder, who has granted bioRxiv a license to display the preprint in perpetuity. It is made available under a CC-BY 4.0 International license.

412 contribute to the regulation of the cell osmotic pressure to meet the need of the change
413 from vegetative to reproductive state. Likewise, Alsufyani et al (2017) investigated
414 that the composition of the metabolites released during Ulva grew under normal
415 conditions with an exo-metabolomic approach and found that higher concentrations of
416 divalent low-molecular metabolites such as maleic and succinic acids were detected in
417 the late gametogenesis phase. An elevated level of organic acid is important for
418 energy production, cellular membrane stabilization, maintenance of turgor,
419 vitrification of cytoplasm and signaling in cells under stress conditions[13,22].
420 Moreover, ascorbic acid is one of the major antioxidant compounds synthesized in
421 plants and used for cell division regulation [23,24]. In orthodox seeds, there is no
422 ascorbic acid and ascorbic acid peroxidase activity in the stationary phase, but they
423 restart after from the onset of imbibition[25]. Many studies have shown that ascorbic
424 acid biosynthesis and rapid restart of ascorbic acid peroxidase activity are the keys to
425 seed germination[26,27]. However, other studies have shown that high doses of
426 ascorbic acid can inhibit the germination of wheat seeds [28]. In this study, 21.43%
427 germ cells were formed at 36h, and 91.57% germ cells were formed at 48 h, and the
428 germ cells started to release in the treatment group. In the meantime, the relative
429 content of ascorbic acid decreased (0.24-fold, at 36h point) and then increased
430 (6.06-fold, at 48h point) compared with those of the control group. In contrast to
431 higher plants, reduced ascorbic acid content in *U. prolifera* may contribute to the
432 formation of germ cells, and higher concentrations of ascorbic acid may contribute to
433 the release of germ cells.

bioRxiv preprint doi: https://doi.org/10.1101/578963; this version posted March 15, 2019. The copyright holder for this preprint (which was not certified by peer review) is the author/funder, who has granted bioRxiv a license to display the preprint in perpetuity. It is made available under a CC-BY 4.0 International license.

Accumulation of GABA is believed to be a redox regulatory mechanism in a variety of terrestrial plants, such as *Arabidopsis* [29], *Lotus japonicus* [30], *Pisum sativum* [29,31] and *Glycine max*[32]. Gallic acid and its related compounds showed significant chromosomal influence characteristics [33,34]. In this study, the relative content of GABA and gallic acid accumulated at 36h in the treatment group, the result was consistent with those of Singh et al.(2016), indicating that these two organic acids played a consistent role in *U. prolifera* and higher plants[23,33-36]

The other metabolites in the formation of germ cells in *U. prolifera*

Compounds constitute phytochemical defense weapons from a variety of metabolic pathways and can be broadly divided into three categories, namely, isoprenoids (e.g., diterpenes), alkaloids (e.g., indole alkaloid camalexin), and shikimates (e.g., flavonoids) [37]. In this study, at 12 h, 2-methyl-3-phenylindole and 3-indoleacetonitrile accumulated in the treatment group (Table 2), suggesting that these metabolites were used for biological defense of *U. prolifera*.

Two obvious changes were noted in alcohol metabolites: glycerol and hexanol (Table 2). The content of glycerol in the treatment group was significantly higher than that in the control group at 60 h after cutting (Fig. 7e). In this study, the Sp of *U. prolifera* was 97% and the Rp was 9.57% at 60 h after cutting, but the they were only 32.86% and zero at 60h in the control group, respectively. Alsufyani et al. (2017) found that the maximum content of glycerol on the surface of *Ulva* was at 21h after

bioRxiv preprint doi: https://doi.org/10.1101/578963; this version posted March 15, 2019. The copyright holder for this preprint (which was not certified by peer review) is the author/funder, who has granted bioRxiv a license to display the preprint in perpetuity. It is made available under a CC-BY 4.0 International license.

455 artificial induction and the glycerol secreted by *U. prolifera* might be the carbon
456 source of its epiphytes. In this experiment, the relative content of glycerol increased
457 significantly at 60h (Fig.7E), which might be the result of the interaction between *U.*
458 *prolifera* and the epiphytes which was beneficial for the formation of the germ
459 cells[38]. Hexanol, a green leaf volatile that can be used as a synergist for insect
460 pheromones, is used for controlling insect populations. In this study, the content of
461 hexanol was not only affected by cutting, but also by photoperiod. The content of
462 hexanol at night (24 h, 48 h, 72 h) was significantly higher than that in the daytime
463 (12 h, 36 h, 60 h), indicating that hexanol might protect *U. prolifera* from nocturnal
464 insect's harm (Fig. 7f). Certainly, further targeted screening for organic acid is
465 necessary to understand the functions of fragmentation-induced proliferation.

466 In conclusion, we found that, after cutting, the reproductive sporangia formed
467 earlier than that in the control group and various of metabolites undergo drastic
468 changes. The kinds of consumed sugars differ significantly at different time points
469 during the formation of sporangium. At the initial stage of proliferation (the first 60 h),
470 the metabolites such as alcohol and organic acid showed significant changes with the
471 photoperiod, which may be the main strategy for *U. prolifera* to cope with adverse
472 environment and rapid proliferation. However, GC-MS approach provides a very
473 preliminary view of the metabolic changes that are the consequences or the causes of
474 the differentiation of the reproductive cells. Identifying effective biomarkers to
475 monitor complex cellular processes in space and time is only the first step before the
476 challenging isolation and structure elucidation of the compound have to be performed

bioRxiv preprint doi: https://doi.org/10.1101/578963; this version posted March 15, 2019. The copyright holder for this preprint (which was not certified by peer review) is the author/funder, who has granted bioRxiv a license to display the preprint in perpetuity. It is made available under a CC-BY 4.0 International license.

in further studies. Besides, bacterial morphogenetic compounds might not be among them, as the biologically active concentration [39-41] seems to be far below the detection limit of the metabolomic approach applied [38]. As (epiphytic) bacteria are essential for *Ulva's* morphogenesis, bacterial compounds are certainly part of the surface-associated metabolome. Future studies will explore these compounds by comparison, e.g., xenic *Ulva* cultures with normally developed adult axenic cultures grown in the presence of purified morphogenetic bacterial compounds[38].

Acknowledgements

We thank the efforts of all people involved in the laboratory work and data analysis, and the collaboration of Dr Wenrong Zhu and Mr. Wei Hu for the donation of *Ulva* samples.

Authors' Contributions

N.X., C.H and Y.H. designed and supervised the research. Y.H. performed experiments, analyzed the data, and wrote the manuscript. Y.W. performed the GC-MS data analysis. All the authors revised and approved the final manuscript.

References

1. Holdt SL (2011) Bioactive compounds in seaweed: functional food applications and legislation. Journal of Applied Phycology 23: 543-597. dio: 10.1007/s10811-010-9632-5.
2. Hiraoka M, Enomoto S (1998) The induction of reproductive cell formation of *Ulva pertusa* Kjellman (Ulvales, Ulvophyceae). Phycol Res 46: 199-203.
3. Dan A, Hiraoka M, Ohno M, Critchley AT (2002) Observations on the effect of salinity and photon fluence rate on the induction of sporulation and rhizoid formation in the green alga *Enteromorpha prolifera* (Müller) J. Agardh (Chlorophyta, Ulvales). Fisheries Science 68: 1182-1188. dio: 10.1046/j.1444-2906.2002.00553.x.
4. Nordby Ø (1977) Optimal conditions for meiotic spore formation in *Ulva mutabilis* FØyn. Bot Mar 20: 19-28. dio:10.1515/botm.1977.20.1.19.

bioRxiv preprint doi: https://doi.org/10.1101/578963; this version posted March 15, 2019. The copyright holder for this preprint (which was not certified by peer review) is the author/funder, who has granted bioRxiv a license to display the preprint in perpetuity. It is made available under a CC-BY 4.0 International license.

5. Gao S, Chen X, Yi Q, Wang G, Pan G, et al. (2010) A strategy for the proliferation of *Ulva prolifera*, main causative species of greentides, with formation of sporangia by fragmentation. PLoS One 5: 199-208. dio: 10.1371/journal.pone.0008571.

6. Nilsen G, ., Nordby O, . (1975) A sporulation-inhibiting substance from vegetative thalli of the green alga *Ulva mutabilis* FØyn. Planta 125: 127-139.

7. Stratmann J, Paputsoglu G, Oertel W (1996) Differentiation of *ulva mutabilis* (cholrophyta) gametangia and gamete release are controlled by extracellular inhbitors. J Phycol 32: 1009-1021.

8. Vesty EF, Kessler RW, Wichard T, Coates JC (2015) Regulation of gametogenesis and zoosporogenesis in *Ulva linza* (Chlorophyta): comparison with *Ulva mutabilis* and potential for laboratory culture. Frontiers in Plant Science 6: 1-8. dio: 10.3389/fpls.2015.00015 Source: PubMed.

9. Coates JC, Umm-E-Aiman, Charrier B (2015) Understanding "green" multicellularity: do seaweeds hold the key? Front Plant Sci 5: 737. dio: 10.3389/fpls.2014.00737

10. Liu XJ, Bogaert K, Engelen AH, Leliaert F, Roleda MY, et al. (2017) Seaweed reproductive biology: environmental and genetic controls. Botanica Marina 2: 89-108.

11. Goulitquer S, Potin P, Tonon T (2012) Mass spectrometry-based metabolomics to elucidate functions in marine organisms and ecosystems. Mar Drugs 10: 849-880. dio:10.3390/md10040849 10.3390/md10040849

12. Gupta V, Thakur RS, Baghel RS, Reddy CRK, Jha B (2014) Seaweed metabolomics: a new facet of functional genomics. Adv Bot Res 71: 31–52.

13. Kumar M, Kuzhiumparambil U, Pernice M, Jiang Z, Ralph PJ (2016) Metabolomics: an emerging frontier of systems biology in marine macrophytes. Algal Research 16: 76-92.

14. Tian H, Lam SM, Shui G (2016) Metabolomics, a powerful tool for agricultural research. Int J Mol Sci 17: 1871.

15. Cui J, Zhang J, Huo Y (2015) Adaptability of free-floating green tide algae in the Yellow Sea to variable temperature and light intensity. Marine Pollution Bulletin, http://dx.doi.org/10.1016/j.marpolbul.2015.10.033.

16. He YL, Hu CY, Wang YH, Cui DD, Sun X, et al. (2018) The metabolic survival strategy of marine macroalga *Ulva prolifera* under temperature stress. J Appl Phycol 30(6): 3611-3621. dio: 10.1007/s10811-018-1493-3.

17. Xia J, Wishart DS (2016) Using MetaboAnalyst 3.0 for comprehensive metabolomics data analysis. Curr Protoc Bioinf 55: 1-91. dio: 10.1002/cpbi.11.

18. Umetrics M (2013) User guide to SIMCA. Malmö (Sweden): MKS Umetrics AB.

19. Xia J, Sinelnikov IV, Wishart DS (2011) MetATT: a web-based metabolomics tool for analyzing time-series and two-factor datasets. Bioinformatics 27: 2455-2456. dio: 10.1093/bioinformatics/btr392.

20. Smeekens S, Ma J, Hanson J, Rolland F (2010) Sugar signals and molecular networks controlling plant growth. Curr Opin Plant Biol 13: 273-278. dio: 10.1016/j.pbi.2009.12.002 · Source: PubMed.

21. Kaplan F, Guy CL (2004) beta-Amylase induction and the protective role of maltose during temperature shock. Plant Physiol 135: 1674-1684. dio: 10.1104/pp.104.040808.

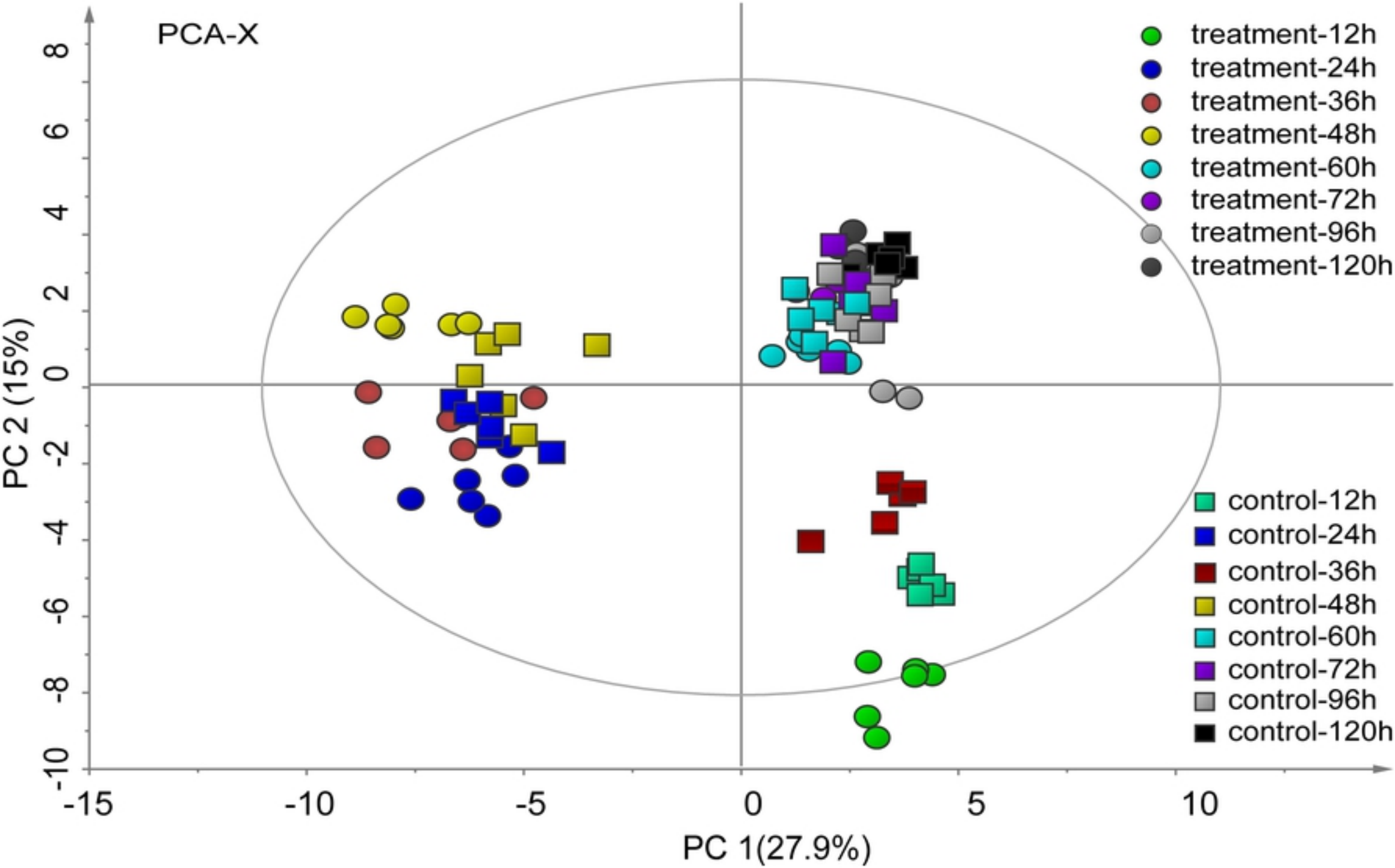
22. Obata T, Fernie AR (2012) The use of metabolomics to dissect plant responses to abiotic stresses. Cellular & Molecular Life Sciences 69: 3225-3243. dio: 10.1007/s00018-012-1091-5.

bioRxiv preprint doi: https://doi.org/10.1101/578963; this version posted March 15, 2019. The copyright holder for this preprint (which was not certified by peer review) is the author/funder, who has granted bioRxiv a license to display the preprint in perpetuity. It is made available under a CC-BY 4.0 International license.

548 23. Ozfidan-Konakci C, Yildiztugay E, Kucukoduk M (2015) Protective roles of exogenously applied
549 gallic acid in *Oryza sativa* subjected to salt and osmotic stresses: effects on the total
550 antioxidant capacity. Plant Growth Regul 75: 219-234. dio: 10.1007/s10725-014-9946-4.
551 24. Kka N, Rookes J, Cahill D (2018) The influence of ascorbic acid on root growth and the root apical
552 meristem in *Arabidopsis thaliana*. Plant Physiology & Biochemistry 129: 232-330. dio:
553 10.1016/j.plaphy.2018.05.031.
554 25. Tommasi F, Paciolla C, Arrigoni O (1999) The ascorbate system in recalcitrant and orthodox seeds.
555 Physiologia Plantarum 105: 193-198. dio: 10.1034/j.1399-3054.1999.105202.x.
556 26. Gara LD, Paciollo C, Liso R, Stefani A, Arrigoni O (1991) Correlation between ascorbate
557 peroxidase activity and some anomalies of seedlings from aged caryopses of *Dasypyrum*
558 *villosum* (L.) Borb. Journal of Plant Physiology 137: 697-700. dio:
559 10.1016/s0176-1617(11)81224-1.
560 27. Gara LdC, De TM, Motto M, Arrigoni O, De GL, et al. (2010) Ascorbate-dependent hydrogen
561 peroxide detoxification and ascorbate regeneration during germination of a highly productive
562 maize hybrid: evidence of an improved detoxification mechanism against reactive oxygen
563 species. Physiologia Plantarum 109: 7-13. dio:10.1034/j.1399-3054.2000.100102.x.
564 28. Ishibashi Y, Iwayainoue M (2006) Ascorbic acid suppresses germination and dynamic states of
565 water in wheat seeds. Plant Production Science 9: 172-175. dio: 10.1626/pps.9.172. dio:
566 10.1626/pps.9.172.
567 29. Dongen JTV, Fröhlich A, Ramírez-Aguilar SJ, Schauer N, Fernie AR, et al. (2009) Transcript and
568 metabolite profiling of the adaptive response to mild decreases in oxygen concentration in the
569 roots of *arabidopsis* plants. Annals of Botany 103: 269-280.
570 30. Marcio R, Francesco L, Araújo WL, Adriano NN, Ladaslav S, et al. (2010) Glycolysis and the
571 tricarboxylic acid cycle are linked by alanine aminotransferase during hypoxia induced by
572 waterlogging of *Lotus japonicus*. Plant Physiology 152: 1501-1513. dio:
573 10.1104/pp.109.150045.
574 31. Ana Z, Luis O, María I, Nicolas S, Fernie AR, et al. (2011) Unraveling the role of fermentation in
575 the mode of action of acetolactate synthase inhibitors by metabolic profiling. Journal of Plant
576 Physiology 168: 1568-1575. dio: 10.1016/j.jplph.2011.02.015.
577 32. Allen DK, Young JD (2013) Carbon and nitrogen provisions alter the metabolic flux in developing
578 soybean embryos. Plant Physiology 161: 1458-1475.
579 33. George EF, Hall MA, Klerk GJD (2007) The components of plant tissue culture media II: organic
580 additions, osmotic and pH effects, and support systems. Berlin: Springer. pp. 115–174.
581 34. Singh R, Singh S, Parihar P, Mishra RK, Tripathi DK, et al. (2016) Reactive oxygen species (ROS):
582 beneficial companions of plants' developmental processes. Frontiers in Plant Science 7. dio:
583 10.3389/fpls.2016.01299.
584 35. White MC (1981) Metal complexation in xylem fluid: I. chemical composition of tomato and
585 soybean stem exudate. Plant Physiology 67: 292-300.
586 36. Gupta V, Kushwaha HR (2017) Metabolic regulatory oscillations in intertidal green seaweed *Ulva*
587 *lactuca* against tidal cycles. Sci Rep 7: 16430. dio: 10.1038/s41598-017-15994-2.
588 37. Balmer D, Flors V, Glauser G, Mauch-Mani B (2013) Metabolomics of cereals under biotic stress:
589 current knowledge and techniques. Front Plant Sci 4: 82. dio: 10.3389/fpls.2013.00082.
590 38. Alsufyani T, Weiss, A., & Wichard, T. (2017) Time course exo-metabolomic profiling in the green
591 marine macroalga *Ulva* (chlorophyta) for identification of growth phase-dependent biomarkers.

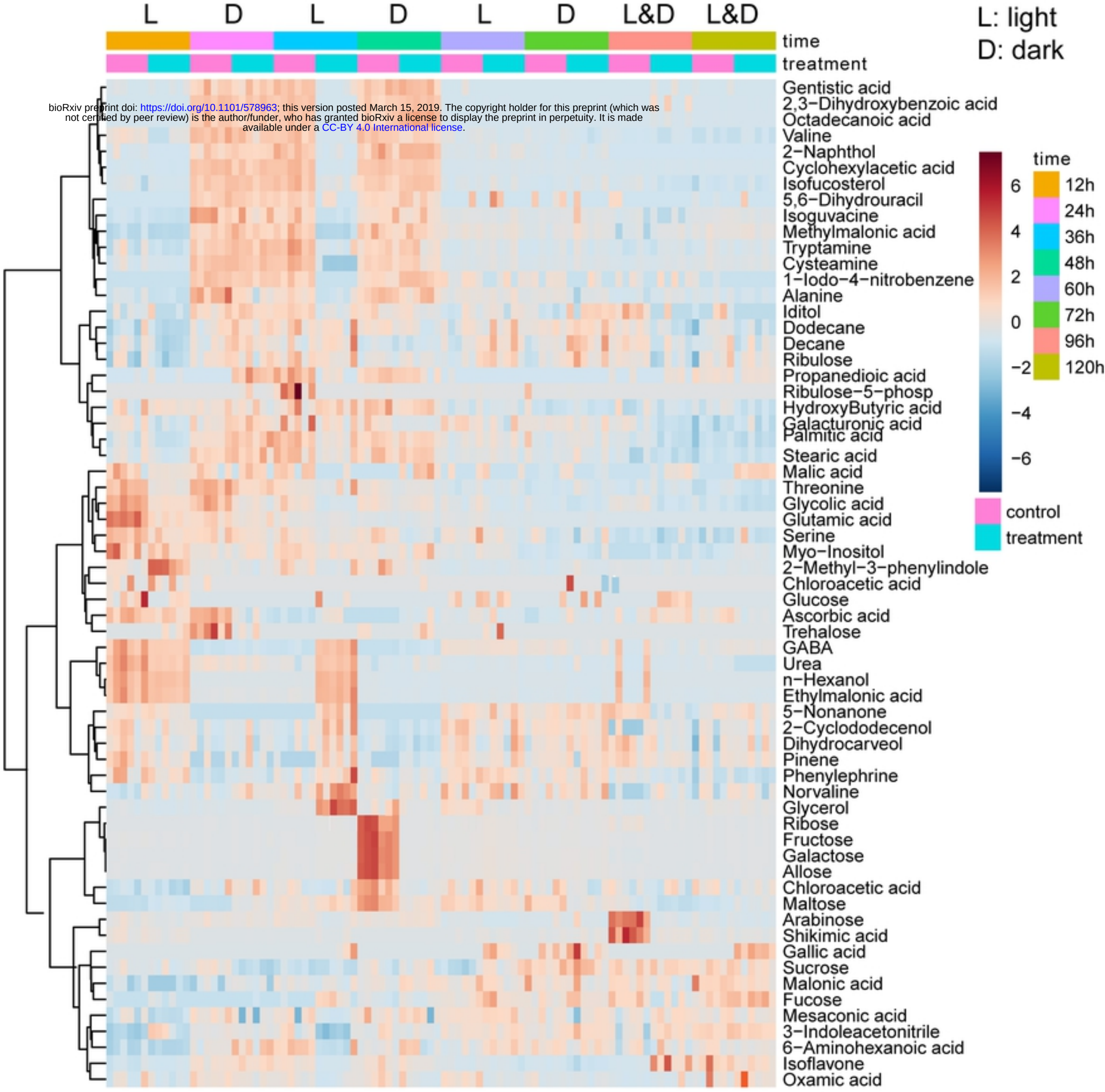
bioRxiv preprint doi: https://doi.org/10.1101/578963; this version posted March 15, 2019. The copyright holder for this preprint (which was not certified by peer review) is the author/funder, who has granted bioRxiv a license to display the preprint in perpetuity. It is made available under a CC-BY 4.0 International license.

592 Marine Drugs 15: 1-20. dio: 10.3390/md15010014.
593 39. Fries L, Āberg S (1978) Morphogenetic effects of phenylacetic and p-OH-phenylacetic acid on the
594 green alga *Enteromorpha compressa* (L.) GREV. in axenic culture. Zeitschrift Für
595 Pflanzenphysiologie 88: 383-388.
596 40. Spoerner M, Wichard T, Bachhuber T, Stratmann J, Oertel W (2012) Growth and thallus
597 morphogenesis of *Ulva mutabilis* (Chlorophyta) depends on a combination of two bacterial
598 species excreting regulatory factors. Journal of Phycology 48: 1433-1447.
599 41. Grueneberg J, Engelen AH, Costa R, Wichard T (2015) Macroalgal morphogenesis induced by
600 waterborne compounds and bacteria in coastal seawater. Plos One 11: e0146307.
601 doi:10.1371/journal.pone.0146307.
602


PCA-X
treatment-12h
treatment-24h
treatment-36h
treatment-48h
treatment-60h
treatment-72h
treatment-96h
treatment-120h
control-12h
control-24h
control-36h
control-48h
control-60h
control-72h
control-96h
control-120h
PC 2 (15%)
PC 1(27.9%)
8
6
4
2
0
-2
-4
-6
-8
-10
-15
-10
-5
0
5
10

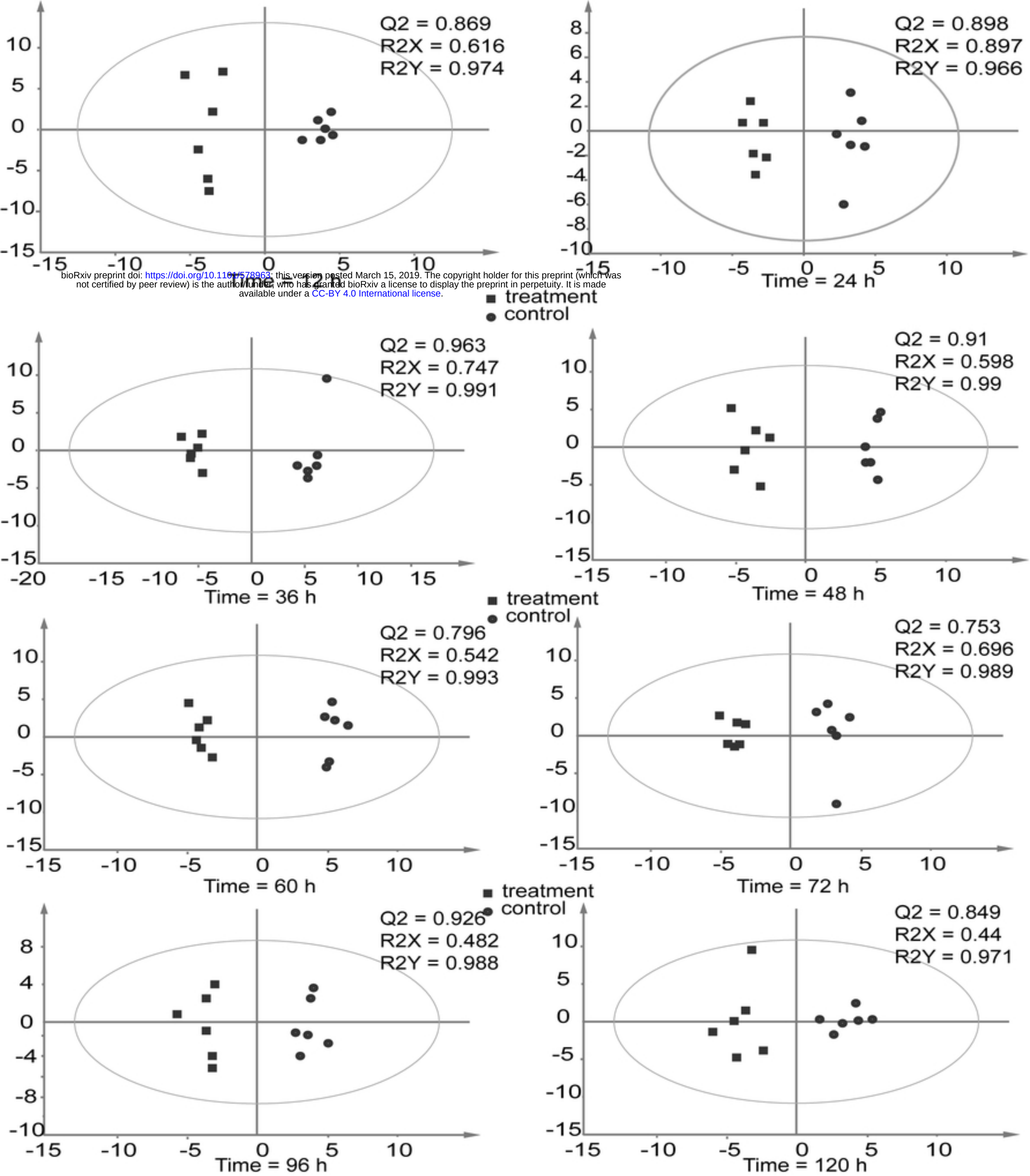
Figure

bioRxiv preprint doi: https://doi.org/10.1101/578963; this version posted March 15, 2019. The copyright holder for this preprint (which was not certified by peer review) is the author/funder, who has granted bioRxiv a license to display the preprint in perpetuity. It is made available under a CC-BY 4.0 International license.

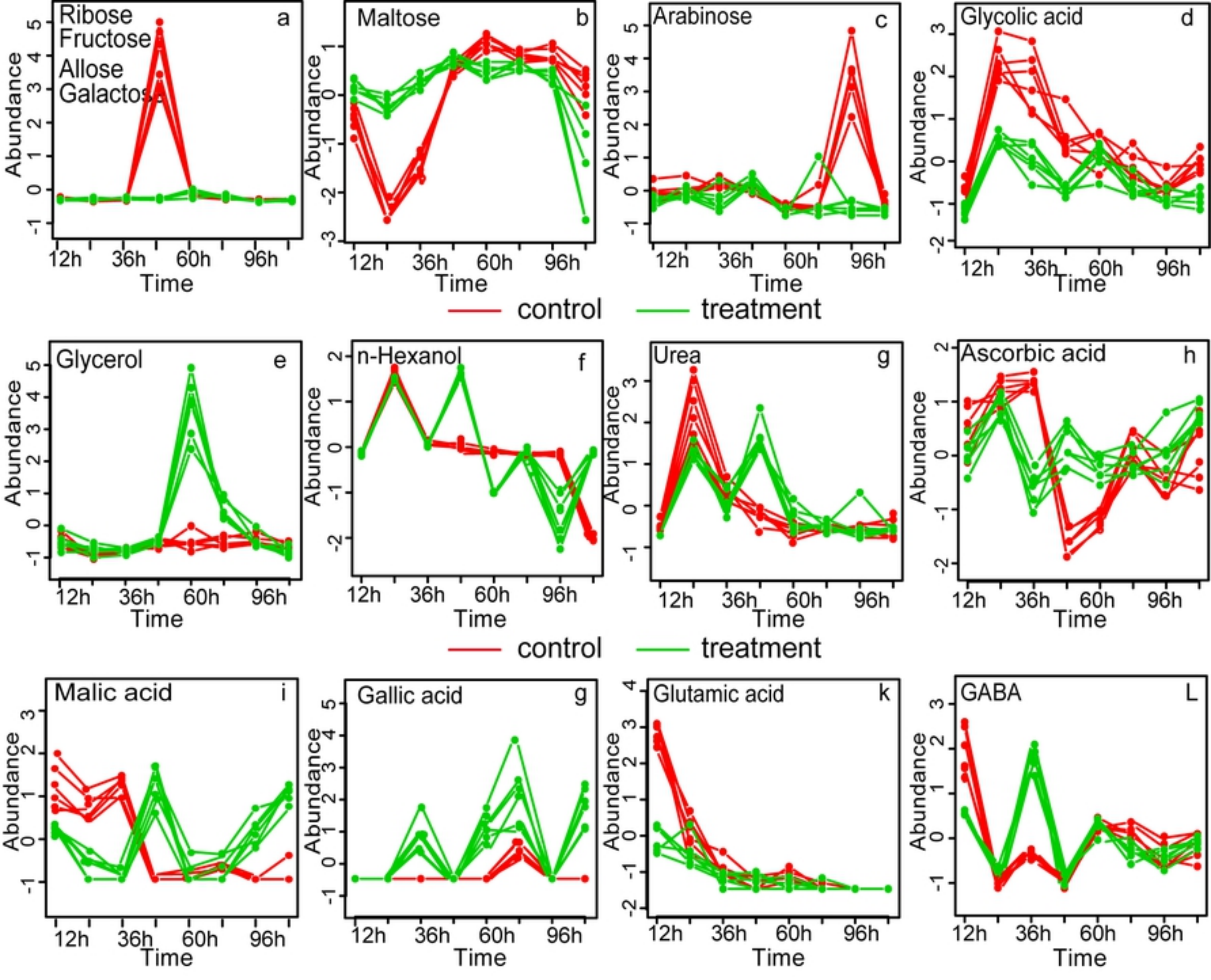


Figure

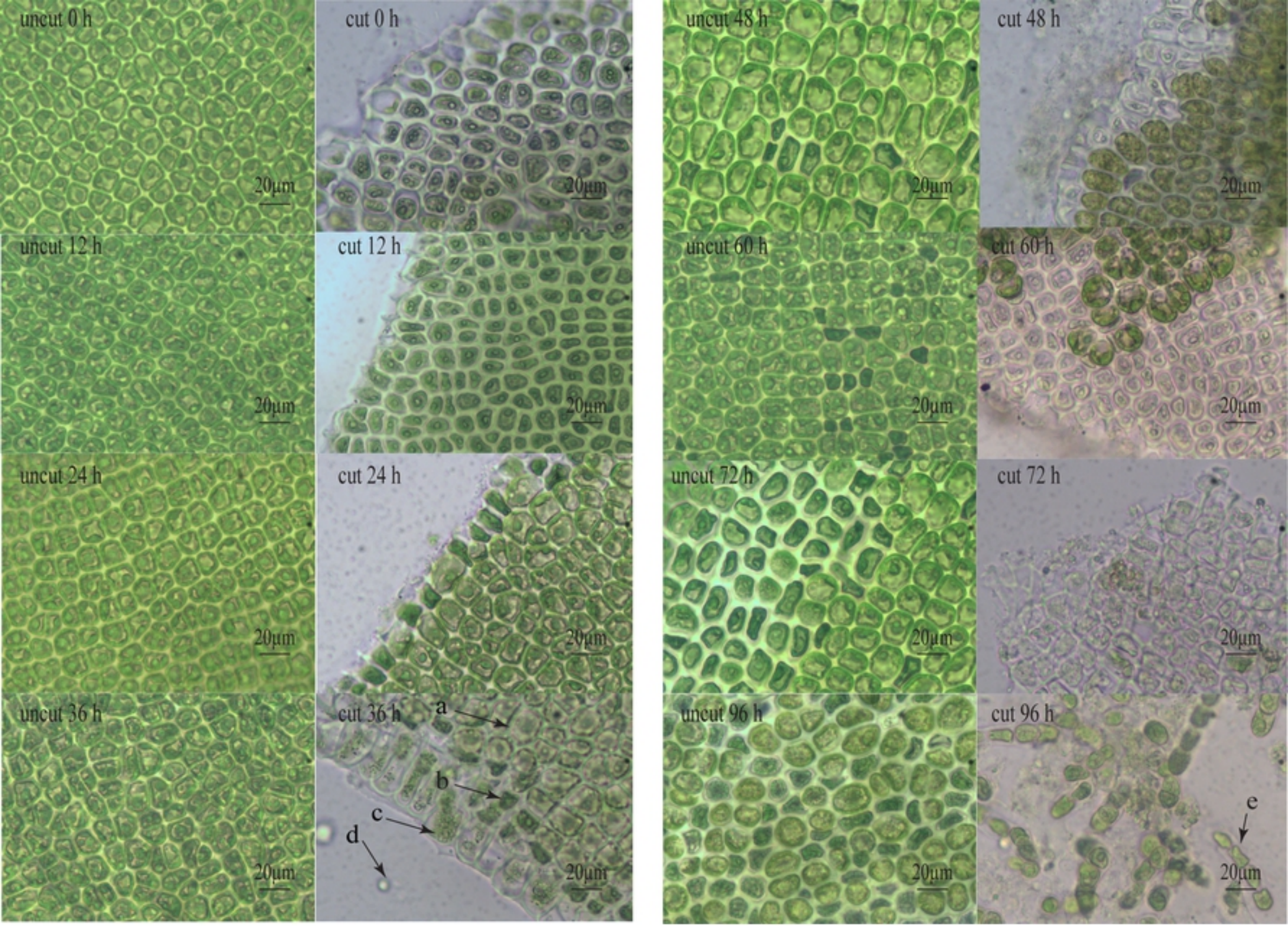
bioRxiv preprint doi: https://doi.org/10.1101/578963; this version posted March 15, 2019. The copyright holder for this preprint (which was not certified by peer review) is the author/funder, who has granted bioRxiv a license to display the preprint in perpetuity. It is made available under a CC-BY 4.0 International license.



Figure

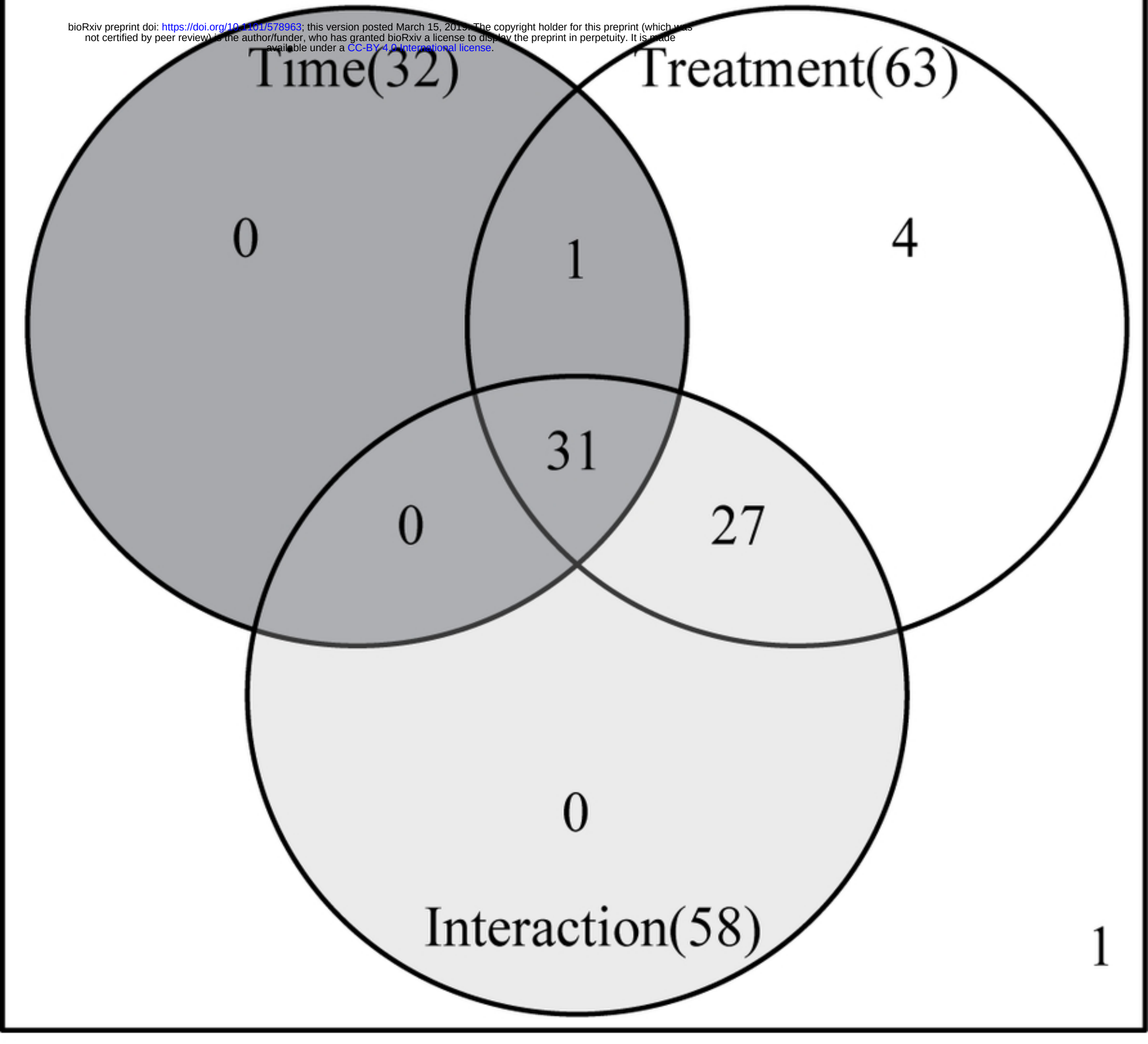

Ribose
Fructose
Allose
Galactose
a
Maltose
b
Arabinose
c
Glycolic acid
d
Abundance
Time
12h
36h
60h
96h
control
treatment
Glycerol
e
n-Hexanol
f
Urea
g
Ascorbic acid
h
Malic acid
i
Gallic acid
g
Glutamic acid
k
GABA
L

Figure

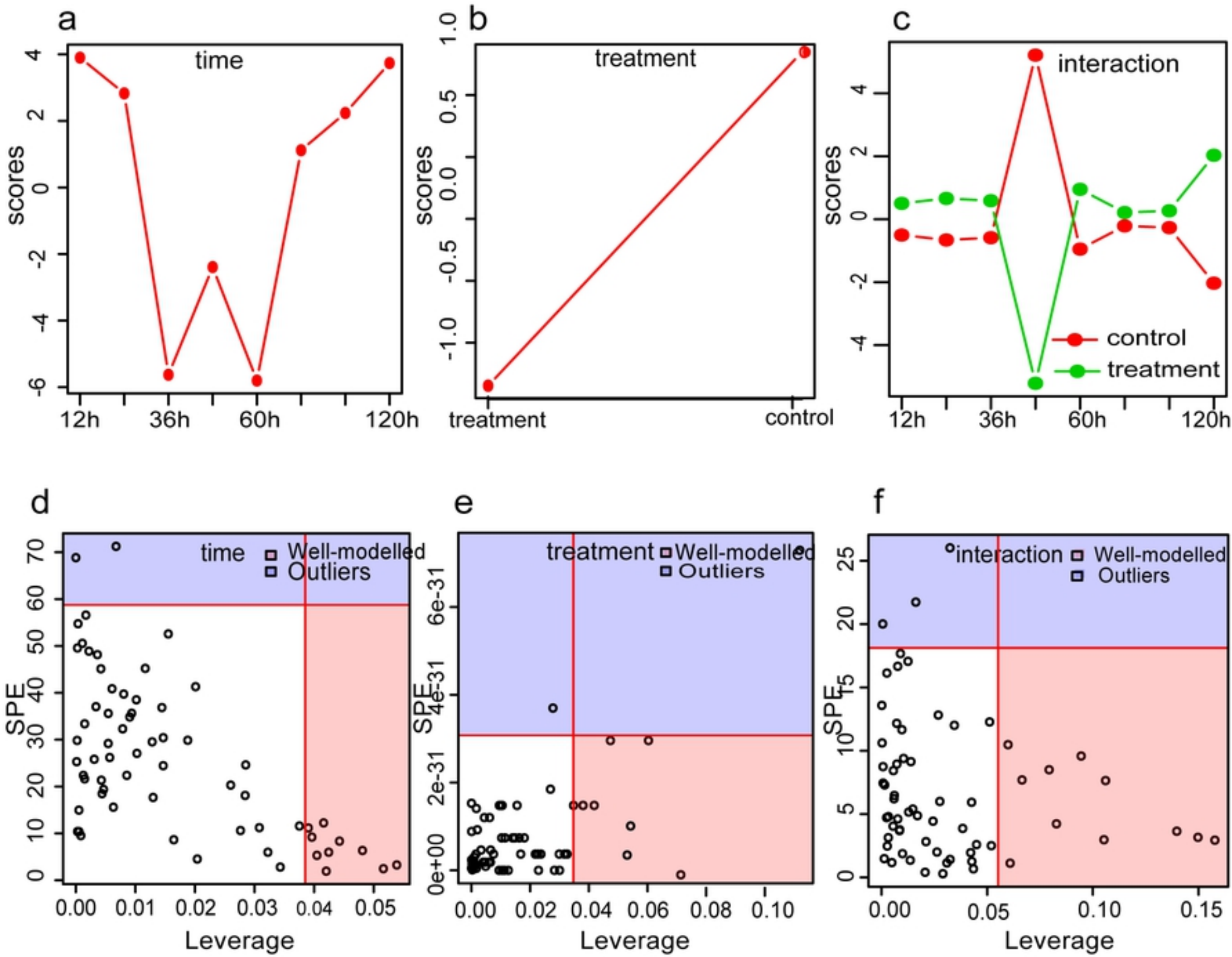

uncut 0 h
cut 0 h
uncut 48 h
cut 48 h
uncut 12 h
cut 12 h
uncut 60 h
cut 60 h
uncut 24 h
cut 24 h
uncut 72 h
cut 72 h
uncut 36 h
cut 36 h
uncut 96 h
cut 96 h
20µm
a
b
c
d
e

Figure

bioRxiv preprint doi: https://doi.org/10.1101/578963; this version posted March 15, 2019. The copyright holder for this preprint (which was not certified by peer review) is the author/funder, who has granted bioRxiv a license to display the preprint in perpetuity. It is made available under a CC-BY-4.0 International license.



Figure


a
time
scores
12h
36h
60h
120h
b
treatment
scores
treatment
control
c
interaction
scores
control
treatment
12h
36h
60h
120h
d
time
Well-modelled
Outliers
SPE
Leverage
e
treatment
Well-modelled
Outliers
SPE
Leverage
f
interaction
Well-modelled
Outliers
SPE
Leverage

Figure